Desalination and Water Treatment
www.deswater.com
doi: 10.5004/dwt.2021.27236

226 (2021) 347–361
June

Efficient removal of Reactive Orange 13 with magnetic *Mucor circinelloides* from mill scale

Pınar Aytar Çelik[a,b], Abdulsamee M.K. Abutaha[b], Belma Nural Yaman[c,*], Hakan Çakmak[b], Seda Hoşgün[d], Ahmet Çabuk[b,e]

[a]*Environmental Protection and Control Program, Eskişehir Osmangazi University, Eskişehir, Turkey, email: pinarytar@gmail.com (P. Aytar Çelik)*
[b]*Department of Biotechnology and Biosafety, Eskişehir Osmangazi University, Eskişehir, Turkey, emails: abod19943911@hotmail.com (A.M.K. Abutaha), hkncakmakk@gmail.com (H. Çakmak)*
[c]*Biomedical Engineering, Eskişehir Osmangazi University, Eskişehir, Turkey, Tel. +90222 239 37 50 – 3182; Fax: +90 222 239 35 78; email: nuralbelma@gmail.com (B. Nural Yaman)*
[d]*Department of Chemical Engineering, Eskişehir Osmangazi University, Eskişehir, Turkey, email: serol@ogu.edu.tr (S. Hoşgün)*
[e]*Department of Biology, Eskişehir Osmangazi University, Eskişehir, Turkey, email: acabuk@ogu.edu.tr (A. Çabuk)*

Received 28 December 2020; Accepted 14 March 2021

ABSTRACT

Mucor circinelloides isolated from mill scale was magnetized by using the method of co-precipitation under alkaline conditions and this magnetized fungus was utilized efficiently to remove reactive textile dyestuff such as Reactive Orange 13. The value of saturation magnetization was obtained 4.93083 emu/g and Brunauer–Emmett–Teller surface area for this untreated magnetic biosorbent and dye-loaded magnetic biosorbent were obtained as 7.88 and 23.25 m^2/g, respectively. After experimental study was carried out, predicted values obtained at 95% confidence interval indicated that the magnetized fungal biomass (1.60 g/L) could adsorb RO13 dyestuff (339.86 ppm) at 34.95°C with a yield of 93.476% (predicted value) in 84.90 min. In these conditions, the experiment was realized, and dye removal was found to be 95.765%. The adsorption kinetic and isotherm of magnetic biosorbent were examined. The results indicated that the adsorption process of Reactive Orange 13 by magnetized fungus was more suitable with Pseudo-second-order kinetic model. The adsorption isotherm was fitted better with Langmuir model. Fourier transform infrared spectroscopy, Raman spectroscopy, X-ray diffraction, and scanning electron microscopy/energy dispersive X-ray spectroscopy analyses were utilized for biosorbent characterization.

Keywords: Magnetic biosorbent; Mill scale; Biosorption

1. Introduction

The most important environmental problem in recent years is caused by the presence of micro-contaminants such as endocrine disruptors, drugs, personal care products, pesticides, and hormones [1]. Other pollutants such as heavy metals and dyes also cause environmental pollution [1,2]. Dyestuffs are also one of the most significant pollutants in the wastewater from different industries [3]. Textile dyes, which are soluble organic compounds, are classified as particularly reactive, direct, basic, and acidic. The biggest damage caused by the textile industry to the environment arises from the discharge of untreated wastewater into water bodies. The dyestuff associated with textile dyes not only

* Corresponding author.

cause aesthetic damage to water bodies, but also prevent light from entering the water, resulting in lower photosynthesis and lower dissolved oxygen levels, which in turn affects all aquatic organisms [4]. Textile dyes also acting as toxic, mutagenic and carcinogenic substances [3–5], are still environmental pollutants and pass through all food chains that provide biomagnification. Therefore, highly trophic level organisms have higher pollution levels than their prey. In this sense, special mention should be made of azo textile dyes that do not combine with fabrics by about 15%–50% during the dyeing process and are released into waste water and are widely used in agricultural irrigation in developing countries. The use of these azo compounds is very detrimental to the soil microbial community and the germination and growth of plants [4]. In recent years, the removal of dyes from effluent has given much attention in managing water contamination [3]. Adsorption is usually determined as cost-effective technique amongst available treatment options. Providing lower toxic by-products and higher efficiency are the most important advantages of adsorption process [6]. Coal, wood, rice husk, fly ash, activated carbon, cotton waste, and clay are used as an adsorbent for the removal of dye from its aqueous solutions [7].

Native or chemically modified fungal biosorbents have been investigated to remove heavy metals or dyestuffs [8–13]. Furthermore, when evaluating many natural and synthetic adsorbents studied in the literature, it is obvious that magnetic compounds (MCs) and magnetic nanocomposites (MNCs) draw attention in removing the dyes from the aqueous solution [3,14,15]. The adaptation of existing adsorbents as MCs/MNCs offers them an outstanding advantage; after adsorption or regeneration, they provide good recovery by magnetic separation technology [16]. The development of special nanoparticles with magnetic properties and high adsorption ability provides a new tool to deal with wastewater treatment. Functionalized magnetic nanoparticles hold promise for detection and separation application [17].

Especially, iron oxide nanoparticles such as magnetite (Fe_3O_4) and maghemite (γ-Fe_2O_3) for magnetic separation have been examined for water treatment owing to their magnetic features (thereby easy separation with magnetic force), easy synthesis, gaining surface functionality, low cost, chemical inert property and low toxicity [18,19]. Magnetically modified beer yeast cells (*Saccharomyces cerevisiae*) were synthesized utilizing water-based magnetic fluid for the biosorption of different water-soluble dyes [20].

In this study, magnetic *Mucor circinelloides* (MagMC) was investigated as biosorbent for removing acidic textile dyestuff such as Reactive Orange 13 (RO13) from aqueous solution. In order to design the experiments, analyse yield results, and subsequently create the mathematical model and optimize conditions, central composite design methodology was used. With the purpose of revealing biosorption mechanism, kinetic and isotherm models were assessed and thermodynamic study was performed. Fourier transform infrared spectroscopy (FTIR), RAMAN, X-ray diffraction (XRD), and scanning electron microscopy/energy dispersive X-ray spectroscopy (SEM-EDS) analyses were used to characterize biosorbent structure.

2. Materials and methods

2.1. Dyestuffs and chemicals

Commercial grade reactive dyestuffs comprising Reactive Orange 12 (RO12), Reactive Orange 13 (RO13), Reactive Blue 49 (RB49), and Reactive Black 8 (RB8) were kindly provided by Sarar Textile M/S (Manufacturer/Suppliers) (Turkey). Before usage, their peak wavelengths at maximum absorbance were recorded. Their chemical structures are shown in Fig. 1.

2.2. Microorganism isolation and screening studies

Each step in experimental design is given in Fig. 2. Fungi were isolated from mill scales derived from an iron and steel industry. The formation rate of mill scale is about 2% of the steel production [21,22]. The result of major and minor element analyses of the mill scale from which the mentioned fungus was isolated is given in the supplementary document (Table S1).

Collection of scale samples in an iron and steel plant in Turkey was done in 1–l sterile bottle. Prior to processing, samples were kept at 4°C. Malt extract broth medium (MEB) was utilized for isolation of fungi. Once fungal growth appeared, they were streaked onto malt extract agar (MEA) medium for purification and plates were incubated 7 d at 30°C. Purified isolates were maintained on MEA slants at 4°C.

Purified fungal liquid seed samples with 4% inoculum amount belonging to five strains (#1, #2, #3, #4, and #5) isolated from mill scale were grown in malt extract broth including 5% scale and two of these fungal strains (#4 and #5 strains) were able to adsorb scale, while other strains could not. As shown in Table 1a, amongst dried biomasses of two fungi (#4 and #5 strains) investigated for RO12, RO13, RB49, and RB8 removal, a fungus isolate (#4 strain) having efficient adsorption character was chosen and obtained as magnetic form of this biosorbent for the study.

To obtain dried biomass for biosorption, these fungi were grown in MEB medium for 7 d, washed with distilled water, filtered and dried in an oven overnight (65°C) and pulverized to 300 μm and stored at +4°C for further experiments.

2.3. Preparation of magnetic biosorbent and vibrating-sample magnetometer analysis

To prepare the magnetic biosorbent, the method of co-precipitation under alkaline conditions was used. For purpose, $FeSO_4{\cdot}7H_2O$ (209 mg) and $FeCl_3{\cdot}6H_2O$ (405 mg) were dissolved in 8 mL of distilled water and the mixture was heated to 80°C [23]. Then 1 mL of NH_4OH solution (25%) was added dropwise and stirring was continued. Finally, 1 g of powdered fungal biosorbent was added and stirred rapidly at the same temperature for 30 min [24]. At the end of the period, the solution cooled to room temperature was washed three times with distilled water and dried at 60°C for 1 d and milled to obtain a magnetic biosorbent in powder form. This magnetic biosorbent has been confirmed to be magnetite-coated by means of magnet separation in the aqueous solution. This biosorbent obtained was used for further optimization studies and stored at +4°C.

Reactive Orange 12

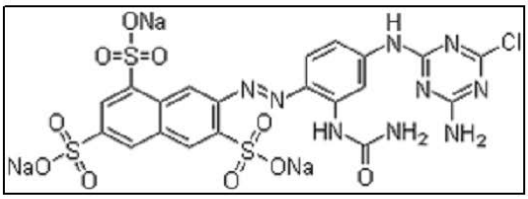

Wavelenght-λ_{max} (nm)	M_a (g/mol)	Structure
418	739.00	Azo

Reactive Orange 13

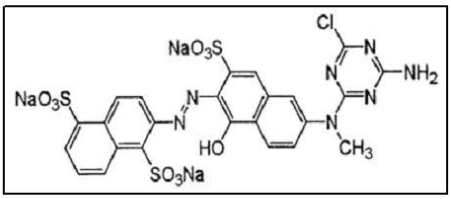

Wavelenght-λ_{max} (nm)	M_a (g/mol)	Structure
488	762.04	Azo

Reactive Blue 49

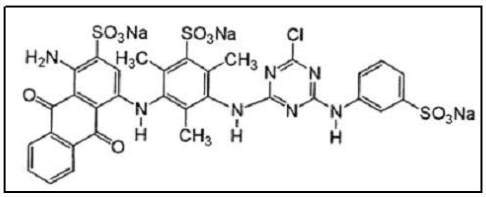

Wavelenght-λ_{max} (nm)	M_a (g/mol)	Structure
587	882.19	Antraquinon

Reactive Black 8

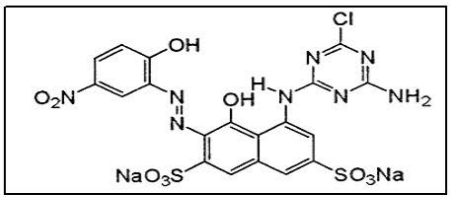

Wavelenght-λ_{max} (nm)	M_a (g/mol)	Structure
547	656.90	Azo, metal komplex

Fig. 1. Characteristics of the dyes given in the study.

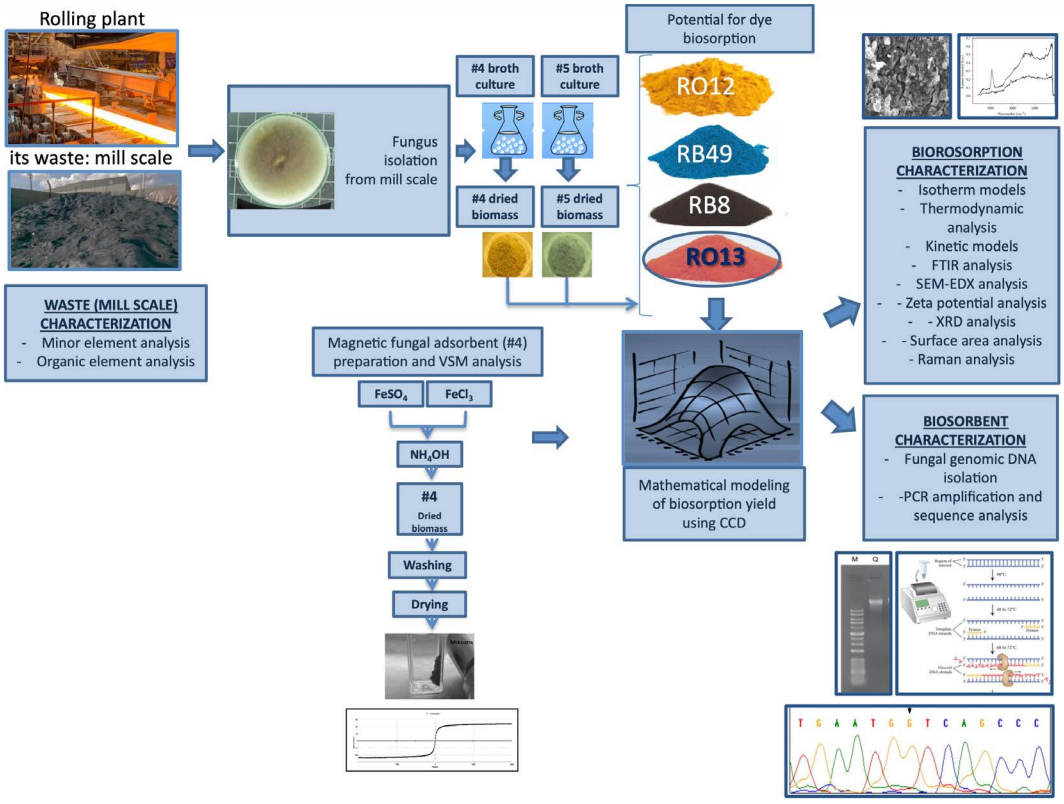

Fig. 2. Schematically experimental procedure.

Table 1
Biosorption capacities of dyestuffs by raw and magnetic fungal biosorbent

(a) Biosorption yield (%) of dyestuffs by #4 and #5 raw fungal biosorbents (working conditions: 50 ppm of initial dye concentration, 150 rev/min of agitation rate, 30°C, 60 min of reaction time, and 1 g/L of biosorbent dosage)

	Biosorption capacities (mg/g)			
	#5 fungal isolate		#4 fungal isolate	
Dyestuff	pH 2	Not adjusted pH (pH 7)	pH 2	Not adjusted pH (pH 7)
RO12	15.585	0	44.745	0
RO13	16.535	0	43.285	0
RB49	24.050	4.555	39.115	0
RB8	16.325	4.060	0.039	0

(b) Biosorption yield (%) of dyestuffs by magnetic biosorbent belonging to #4 fungal strain (working conditions: 150 rev/min of agitation rate, 30°C, 60 min of reaction time, and 1 g/L of biosorbent dosage)

Dyestuff	Biosorption capacities (mg/g)					
	50 ppm		200 ppm		500 ppm	
	pH 2	Not adjusted pH (pH 7)	pH 2	Not adjusted pH (pH 7)	pH 2	Not adjusted pH (pH 7)
RO12	45.315	6.49	31.415	0.42	12.245	0
RO13	46.930	1.61	33.865	0.09	10.545	0

In addition, the magnetic property of this fungal biosorbent was determined by vibrating-sample magnetometer (VSM) at 300 K. This analysis was experimentally plotted with magnetization curve. Analyses were measured with the LakeShore VSM7407 device at a speed of 20 Oe/s in a magnetic field range of ±20 kOe = ramp rate (Fig. 3).

2.4. Biosorption experiments

For batch biosorption, 250 mL Erlenmeyer flasks containing 50 mL working volume of dyestuff solution at 150 rpm and pH 2 was studied. Experiments were designed following the central composite design (CCD) method. Initial dye concentration, biosorbent dosage, reaction period, temperature, and their relationship to the biosorption yield (%) of RO13 dyestuff were expressed in mathematical models. Experimental design and modelling were carried out with Design Expert 10.0.6. Considering the orthogonal quadratic design, the α value was considered to be 2 during calculation of the axial points. Preliminary experiments used to determine independent parameters and levels were given in Table 1b. Independent parameters analysed and their levels are given in Table 2. To assess parameter effects, 30 tests composed of 16 factorial points, 8 axial, and 6 middle points were carried out randomly.

After all experiments finalized, the biosorbents were separated by a magnet and the absorbances of supernatants were measured to define the residual dyestuff concentration at the previously determined wavelengths of each dyestuff using an UV/VIS spectrophotometer (Shimadzu UV2550, Japan). These absorbances were then compared with a standard curve plotted using different concentrations of the dyestuff. Eqs. (1) and (2) were utilized to compute the percentage of decolorization and the biosorption capacity (Q):

$$\%\text{Decolorization} = \frac{C_0 - C_e}{C_0} \times 100 \tag{1}$$

$$q = V \times \frac{C_0 - C_e}{m} \tag{2}$$

where C_0 is the initial concentration (mg/L) of dyestuff, C_e is the equilibrium concentration (mg/L) of dyestuff at the optimization stage, V is the volume of the dyestuff solution (L), and m is the amount of biosorbent (g).

Based on a quadratic model, the results from the experiments were subjected to a variance analysis and using the 95% CI, a backward elimination methodology enabled the deletion of terms not significant. Then, the reduced model was provided.

2.5. Thermodynamic studies

Thermodynamic studies were performed under the previously determined optimal conditions. The prepared samples were incubated in medium with pH 2 at 25°C, 30°C, 35°C and 150 rpm for 60 min. At the end of this period, absorbance values were read and $\Delta G°$, $\Delta H°$, and $\Delta S°$ values were calculated using experimental results. Isotherms are generally used to describe adsorption. Among the two commonly applied isotherms, Freundlich isotherm [Eq. (3)] is described as:

$$q_e = K_F \times C_e^n \tag{3}$$

Langmuir isotherm [Eq. (4)] is described as:

$$\frac{C_e}{q_e} = \frac{1}{\left(bq_m\right)} + \frac{1}{q_m} C_e \tag{4}$$

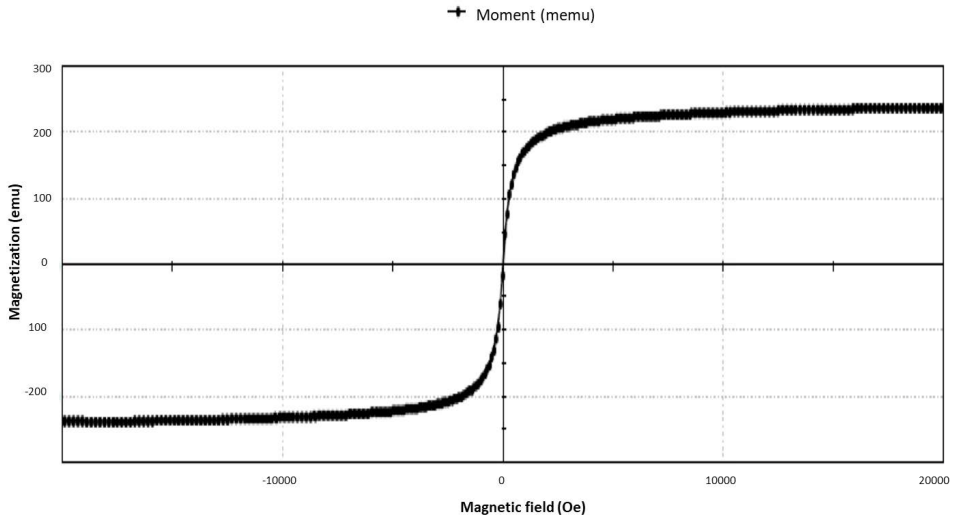

Fig. 3. Magnetization curve of magnetic fungal biosorbent.

In Eq. (4), q_e describes the amount of dye adsorbed per unit mass of the adsorbent, C_e describes the equilibrium concentration of dye, K_F and n are the Freundlich coefficient. The adsorption coefficient was found by Linear Freundlich plots of logq_e vs. logC_e. Some analysis of the Langmuir equation related basis of a dimensionless equilibrium parameter, R_L value (known as separation factor) which is generally seen to indicate adsorption more reliably [25] given by the following equation:

$$R_L = \frac{1}{\left(1+bC\right)} \tag{5}$$

In Eq. (5), b is Langmuir equilibrium coefficient and C is any adsorptive concentration at which the adsorption is carried out. R_L value evaluated for favourable adsorption, $0 < R_L < 1$, while $R_L > 1$ means unfavourable adsorption process. R_L = 1 value represents linear adsorption and R_L = 0 value indicates that the adsorption process is irreversible.

The thermodynamic parameters, ΔG, ΔH, and ΔS for the adsorption process are computed as follows:

$$\ln K_d = \frac{\Delta S}{R} - \frac{\Delta H}{RT} \tag{6}$$

$$\Delta G = \Delta H - \Delta S \tag{7}$$

where K_d in Eq. (6) is termed the distribution coefficient (q_e/C_e). The slope and intercept of the linear plot of lnK_d vs. $1/T$ can be used to compute ΔH and ΔS. With using ΔH and ΔS values, ΔG was calculated according to Eq. (7) [26].

2.6. Kinetic studies

Kinetic studies were performed at various time intervals, at different temperatures (25°C–30°C–35°C), at pH 2 and an initial dye concentration of 240 ppm in the batch system to know when it reached sorption equilibrium. The amount of dye adsorbed was computed from the difference between the initial and equilibrium concentration and results were evaluated with Lagergren's pseudo-first-order kinetic model and pseudo-second-order kinetic model.

The first-order kinetic model generally expressed as:

$$\ln C_t = \ln C_i - k_1 t \tag{8}$$

where C_t (mg/L) is the dye concentration at time t (min), C_i (mg/L) is the initial dye concentration, k_1 (min^{-1}) is the rate constant. The plot of ln(C_t) vs. time (t) was a straight line suggesting a first-order kinetics. Most systems responding to second-order kinetics model for sorption reactions, are generally represented by the equation:

$$\frac{dq_t}{dt} = k_2\left(q_e - q_t\right)^2 \tag{9}$$

where k_2 defines the rate of pseudo-second-order adsorption and q_e and q_t represent the amount of dye adsorbed at equilibrium and the amount adsorbed at any time respectively. The sorption rate can be calculated as the initial sorption rate when t approaches zero. The pseudo-second-order equation can be written as:

$$\frac{t}{q_t} = \frac{1}{k_2 q_e^2} + \frac{t}{q_e} \tag{10}$$

The slope and intercept of the linear plot of t/q_t to t produced k_2 and q_e, respectively, as already defined in Eq. (10).

2.7. Biosorption characterization

2.7.1. FT-IR analysis

In this study, FTIR analyses determined the possible groups that could interact with the RO13 dyestuff on the surface of the #4 fungal biosorbent used as adsorbent after the biosorption process. For FT-IR analysis, untreated

magnetic biosorbent and dye loaded biosorbent samples were pressed into disk by mixing 1% with potassium bromide. The FT-IR spectra of the discs were taken at 400–4,000 cm^{-1}. FT-IR spectroscopy was performed on Bruker Tensor 27.

2.7.2. Raman analysis

In this study, Raman spectroscopy analysis was performed in order to obtain information about magnetic fungal biosorbent structures both before and after biosorption and to determine if there is a change in the structure after adsorption. In addition, it was aimed to obtain information about whether $FeCl_3$ and $FeSO_4$ compounds, which are effective in becoming magnetic, attach to the biosorbent and the structure of the new magnetic biosorbent. For this purpose, Raman analysis was performed using Renishaw INVIA brand Raman spectroscopy at 100–4,000 cm^{-1} spectrum range, 532 nm wavelength laser is used, the spectral scanning at 4 cm^{-1} intervals was performed.

2.7.3. Zeta potential analysis

To determine the pH_{PZC} point of the magnetic biosorbent, 100 mL of distilled water was added to the flasks and the pH was adjusted to 1.0–12.0 with HCl or NaOH. Magnetic biosorbents were placed in each flask at a concentration of 1 g/L to form a colloidal system and the mixture was stirred and waited for 5 min to stabilize the colloidal system. Then, the zeta potentials of these colloidal systems at different pHs were measured and their surface loads were determined. The zeta potential was measured by using a Zetasizer Nano ZS (Malvern Instrument, Ltd., U.K.).

2.7.4. XRD analysis

XRD analyses of both raw and magnetic biosorbent were performed in Panalytical EMPYREAN XRD device and structural changes were revealed.

2.7.5. Surface area analysis

Surface area analyses of both raw biosorbent and magnetic biosorbent were performed with Quantachrome NOVA TOUCH LX4 model device.

2.7.6. SEM-EDX analysis

In order to investigate the surface behaviour of biosorbent, the physical properties of raw and dye loaded biosorbent surfaces were obtained by using SEM (JEOL 560 LV SEM) combined with elemental analyser. The magnetic modification on the biosorbent was evaluated by energy diffraction X-ray (EDX) analyses of both the non-magnetic raw biosorbent and the magnetic fungal biosorbent.

2.8. Biosorbent characterization

2.8.1. Fungal genomic DNA isolation

Genomic DNA isolation from the fungus was done using the CTAB protocol [9]. To check for the presence of DNA, 2 μL of sample was loaded onto a 0.1% agarose gel and run in 1X TAE buffer. 1 kb Plus DNA Ladder (Invitrogen) was used as a marker. Gel photographs were obtained with Biorad Gel Documentation System.

2.8.2. PCR amplification and sequence analysis

The fungal internal transcribed spacer (ITS1-5,8S rDNA region) was amplified using ITS1 (5′-TCCGTAG GTGAACCTTGCGG-3′) and ITS4 (5′-TCCTCCGCTT ATTGATAT GC-3') primer pair. The PCR amplification was carried out in 25 μL reaction mix containing 1× PCR buffer, 25 mM $MgCI_2$, 0.2 mM dNTP, 1.25-unit *Taq* DNA polymerase, 1.2 mM of primer, and 1 μL DNA template. The PCR program comprised of initial denaturation step at 95°C for 5 min, followed by 35 cycles of 95°C for 30 s, 57°C for 1 min, 72°C for 1.5 min followed by a final extension step at 72°C for 10 min [27]. Purification of PCR products was followed sequence analysis whereby similarities were obtained using the BLAST tool from the National Center for Biotechnology Information.

3. Results and discussion

3.1. Screening studies

Table 1a indicates biosorption capacities of dyestuffs by raw fungal biosorbents. According to Table 1, the experiments carried out with 50 ppm of initial dyestuff concentrations for both biosorbents (#4 and #5) showed that #4 fungal biosorbent had better dyestuff biosorption potential than #5 biosorbent. Therefore, further experiments were continued with #4 fungal biosorbent.

Table 1b showed biosorption capacities of dyestuffs by magnetic biosorbent belonging to #4 coded fungal strain. In experiments performed with magnetic biosorbent, biosorption efficiency of RO13 dye was found to be higher level. After the screening studies, experiments were continued with magnetic #4 fungal biosorbent and RO13 dyestuff.

3.2. Mathematical modeling with CCD

3.2.1. Effects of parameters on biosorption

The experiments were applied to the RO13 dyestuff by the fungal biosorbent which had been magnetized, initial dyestuff concentration, biosorbent dosage, reaction period, and reaction temperature were studied as parameters. Previous studies were used to determine the levels. The results from the experiments performed in accordance to the design matrix are given in Table 2. Within the scope of experiments in the design matrix, biosorption yield (%) was calculated for each experimental set and evaluated as a response.

As indicated in Table 3, variance analysis was carried out after obtaining the response values of the experiment sets. An analysis of variance was carried out to examine the linear and quadratic effects of all parameters and a model was created. Since the confidence interval was chosen as 95% in the analysis of variance, the terms with *p*-value less than 0.05 were considered statistically significant in the

Table 2
Design matrix and results of experiments

	Parameters					
Std.	*A*: Initial dye concentration (ppm)	*B*: Biosorbent dosage (g/L)	*C*: Reaction period (min)	*D*: Temperature (°C)	Response: (biosorption yield-%)	*q* (capacity) (mg/g)
1	140	0.6	35	25	60.0979	146.0114
2	340	0.6	35	25	28.6045	156.6952
3	140	1.6	35	25	90.4820	84.89216
4	340	1.6	35	25	69.0408	141.8269
5	140	0.6	85	25	85.3097	207.265
6	340	0.6	85	25	39.0061	213.6752
7	140	1.6	85	25	99.7209	86.84194
8	340	1.6	85	25	87.3737	179.4872
9	140	0.6	35	35	70.1566	189.886
10	340	0.6	35	35	29.6256	195.1567
11	140	1.6	35	35	92.5982	86.73511
12	340	1.6	35	35	71.6412	147.1688
13	140	0.6	85	35	86.9156	237.8917
14	340	0.6	85	35	47.7270	245.0142
15	140	1.6	85	35	99.9663	87.05562
16	340	1.6	85	35	94.2128	193.5363
17	40	1.1	60	30	99.8900	38.81119
18	440	1.1	60	30	46.6744	191.1422
19	240	0.1	60	30	17.4361	401.7094
20	240	2.1	60	30	99.8691	110.2236
21	240	1.1	10	30	41.0339	90.13209
22	240	1.1	110	30	89.0356	186.4802
23	240	1.1	60	20	66.7767	139.8601
24	240	1.1	60	40	83.8419	175.6022
25	240	1.1	60	30	83.0999	174.0482
26	240	1.1	60	30	84.5839	177.1562
27	240	1.1	60	30	78.8336	165.1127
28	240	1.1	60	30	78.0917	163.5587
29	240	1.1	60	30	79.5756	166.6667
30	240	1.1	60	30	81.9870	171.7172

ANOVA table. The correlation values of the biosorption yield of the #4 fungal biosorbent are also given in Table 3.

According to the analysis of variance for the yield of RO13 dyestuff biosorption by fungal biosorbent, the quadratic model was found to be significant. In addition, below the variance analysis table, R^2 and adjusted R^2 values indicating the ratio of model to represent the experiments are given in Table 3. The approximation of the adjusted R^2 value to the R^2 value reveals the power of the model.

The graph showing the changes caused by the affected factors alone in the biosorption yield is given in Fig. 4a with coded parameter levels. As can be seen from Fig. 4a, it is seen that parameters *A* (initial dye concentration), *B* (biomass dosage), and *C* (reaction period) are more effective on dye removal than *D* (reaction temperature) parameter. When factor *A* had a linear effect ($pA < 0.05$ and $pA^2 > 0.05$), both the linear and parabolic effects of *B* and *C* factors were found to be significant. The three-dimensional graph of the initial dye concentration (*A*)-biosorbent dosage (*B*) interaction from the dual interactions is given in Fig. 4b. When the coded factors are considered at the end of the analysis, the resulting model is given in Eq. (11):

$$y = 78.98 - 13.52 \times A + 17.60 \times B + 9.33 \times C + 2.81 \times D + 6.06 \times A \times B - 4.68 \times B^2 - 3.08 \times C^2 \quad (11)$$

3.2.2. Prediction and optimization

Predicted values obtained at 95% confidence interval indicated that magnetic fungal biosorbent (1.60 g/L) could adsorb RO13 dyestuff (339.86 ppm) at 34.95°C with a yield of 93.476% in 84.90 min. In these conditions, the mentioned experiment set was realized and dye removal was found to be 95.765%. The fact that this value remains within the 95% confidence interval and in particular its closeness to

Table 3
Variance analysis for biosorption yield, correlation values, and verification experiment

Variance analysis			
Source	*p*-value Prob. > *F*		Model coefficients for coded values
Model	<0.0001	Significant	+78.98
A-Initial dyestuff concentration (ppm)	<0.0001		–13.52
B-Biosorbent dosage (g/L)	<0.0001		+17.60
C-Reaction period (min)	<0.0001		+9.33
D-Reaction temperature (°C)	0.0116		+2.81
AB	<0.0001		+6.06
B^2	<0.0001		–4.68
C^2	0.0033		–3.08
Lack of fit	0.0512	Not significant	

Correlation values	
R^2	0.9658
pR^2	0.9102
Adj. R^2	0.9549

Verification experiment							
Initial dye concentration (ppm)	Biosorbent dosage (g/L)	Reaction period (min)	Reaction temperature (°C)	95% CI low	Pred. value	95% CI high	Exp. value
339.86	1.60	84.90	34.95	88.15	93.476	98.80	95.767

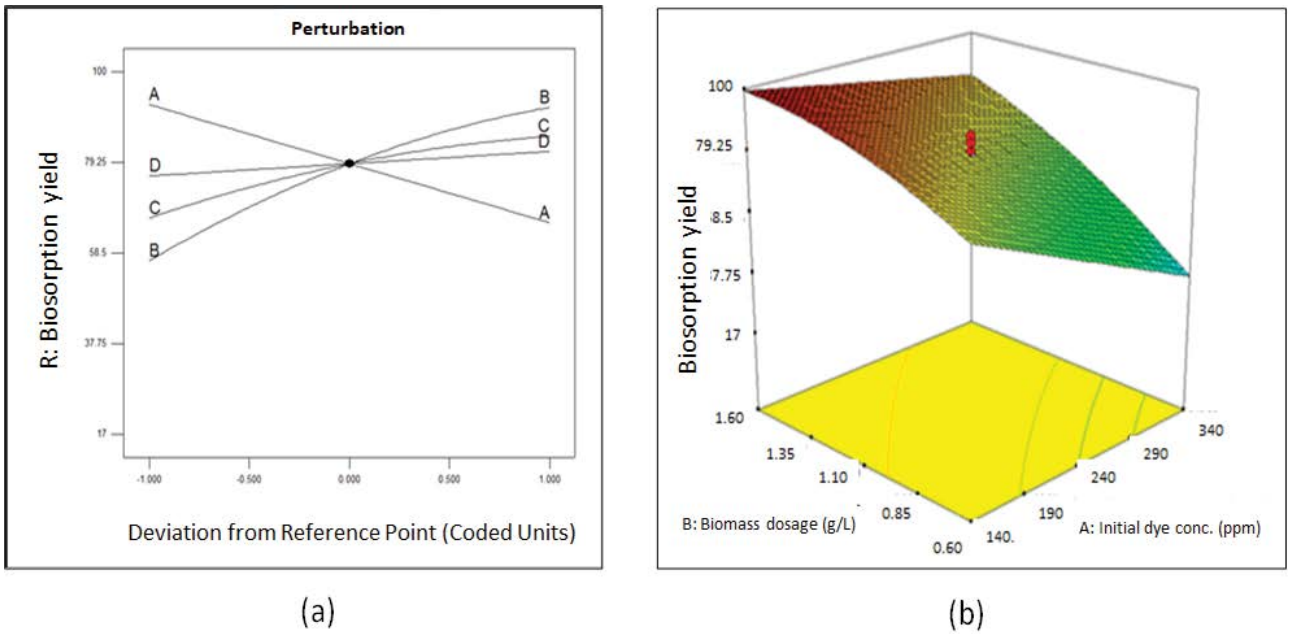

Fig. 4. (a) Main effects of variables on the responses for biosorption yield and (b) the response surface of double interaction of biosorbent dosage and initial dye concentration for biosorption yield.

the predicted value – 93.476% – shows the reproducibility of the experiments and the predictive power of the model; therefore, the success of the model has occurred (Table 3). In similar studies with using of Fe-BDC MOF adsorbent, maximum dye removal was obtained as 94.74% after 24 h [7].

3.3. Thermodynamic and kinetic studies

Equilibrium and kinetics are the key aspects during adsorption. The adsorption isotherm of MagMC for RO13 at 25°C, 30°C, and 35°C and kinetic parameters were calculated

by using the change of dye concentration as a function of time at various temperature and the results were shown in Table 4.

When the temperature is constant, the relationship between the dye uptake and the sorbate equilibrium is referred to as the adsorption isotherm. Several expressions are used to describe adsorption isotherms [28], Langmuir and Freundlich models as the most applied models at dye removal were used in this study. It could be observed from the fitting coefficient R^2 that comparing with Freundlich, Langmuir model was more suitable for this biosorption process (Table 4). This model shows the biosorption with MagMC belonged to the monolayer adsorption. R_L value at 25°C changes between 0.280 and 0.34, at 30°C changes between 0.239 and 0.027 and at 35°C changes between 0.177 and 0.019 shows the biosorption process suitable for this dye-adsorbate complex. Similar studies have seen in the literature [29].

The sorption process's calculated thermodynamic parameters are indicated in Table 4. The positive value of $\Delta H°$ established the endothermic characteristic of biosorption process dye onto MagMC. The experiments investigated temperature effect also indicated that the biosorption capacity increased with increasing medium temperature. q-values are 196.08 mg/g at 25°C and 212.77 mg/g at 35°C (Table 4). The value of $\Delta S°$ was positive which reflects the affinity of magnetic biosorbent toward used dye, and the value of $\Delta G°$ was negative showing how feasible the biosorption process is and its spontaneity.

The use of different kinetic models served to illustrate the dye biosorption with MagMC computed q_e values with pseudo-second-order model highly agreed with data from the experiments and also regression value indicated (Table 4).

3.4. Characterization of biosorption

3.4.1. FTIR analysis

The FT-IR spectra of magnetic biomass and loaded fungal biomass were used to detect biosorption sites as shown in Fig. 5. Magnetic fungal biomass has specific bands which are at 3,433.23; 3,006.97; 2,925.96; 2,584.59; 1,743.62; 1,633.68; 1,080.12; 1,035.75; and 403.11 cm^{-1}. The absorption bands of the O–H stretching, N–H stretching, C=O stretching, C=C stretching, N–O stretching, C–H group, S=O stretching, and C–O group were varieties for dyestuff loaded magnetic fungal biomass.

The band at 1,163.05 cm^{-1} within the FTIR spectrum of dyestuff loaded magnetic fungal biomass was shown that the presence of S=O stretching; but this group band was observed at 1,157.72 cm^{-1} in the magnetic fungal biomass. C–H methylene group was observed at 1,462.01 cm^{-1} in the dyestuff loaded magnetic fungal biomass, however, this band was disappeared in the magnetic fungal biomass. The bands at 898–651 cm^{-1} observed after biosorption were emphasized to biosorption characteristics for aromatic skeletal groups. Furthermore, the band at 651.93 cm^{-1} was only indicated in the dyestuff loaded magnetic fungal biomass.

3.4.2. Raman analysis

Structural analysis of magnetic biosorbent was also performed by Raman spectroscopy. The Raman analyses of $FeCl_3$ and $FeSO_4$ compounds in the literature and in our study are similar to each other. In the Raman analysis of $FeCl_3$, characteristically 500 cm^{-1} vibration, Cl_2 vibration, isotopic vibrations between 300 and 400 cm^{-1} and

Table 4
Isotherm model constants, correlation coefficients, thermodynamic, and kinetic parameters of RO13 biosorption by magnetic fungal biosorbent

Isotherm model constants and correlation coefficients of RO13 biosorption by magnetic fungal biosorbent							
T (°C)	Langmuir isotherm model				Freundlich isotherm model		
	q (mg/g)	b	R^2	$R_{L(10–200)}$	K_F	n	R^2
25	196.08	0.064	0.995	0.280–0.034	77.980	526.32	0.469
30	204.08	0.079	0.999	0.239–0.027	81.433	500.00	0.473
35	212.77	0.116	0.994	0.177–0.019	84.295	454.55	0.517
Thermodynamic parameters of RO13 biosorption by magnetic fungal biosorbent							
T (°C)	$\Delta G°$ (kJ mol^{-1})				$\Delta H°$ (kJ mol^{-1})	$\Delta S°$ (kJ mol^{-1} K^{-1})	
25	–6.878						
30	–6.234				45.309	128.96	
35	–5.589						
Kinetic parameters of RO13 biosorption by magnetic fungal biosorbent							
T (°C)	Pseudo-first-order				Pseudo-second-order			
	k_1 (min^{-1})	q_e (mg/g)	R_1^2	q_{ex} (mg/g)	k_2 (g mg^{-1} min^{-1})	q_e (mg/g)	R_2^2	q_{ex} (mg/g)
25	0.0235	117.30	0.994	179.52	2.673×10^{-4}	204.08	0.993	179.526
30	0.0242	111.97	0.980	184.11	3.138×10^{-4}	204.08	0.996	184.110
35	0.0244	113.42	0.984	186.40	3.092×10^{-4}	208.33	0.996	186.401

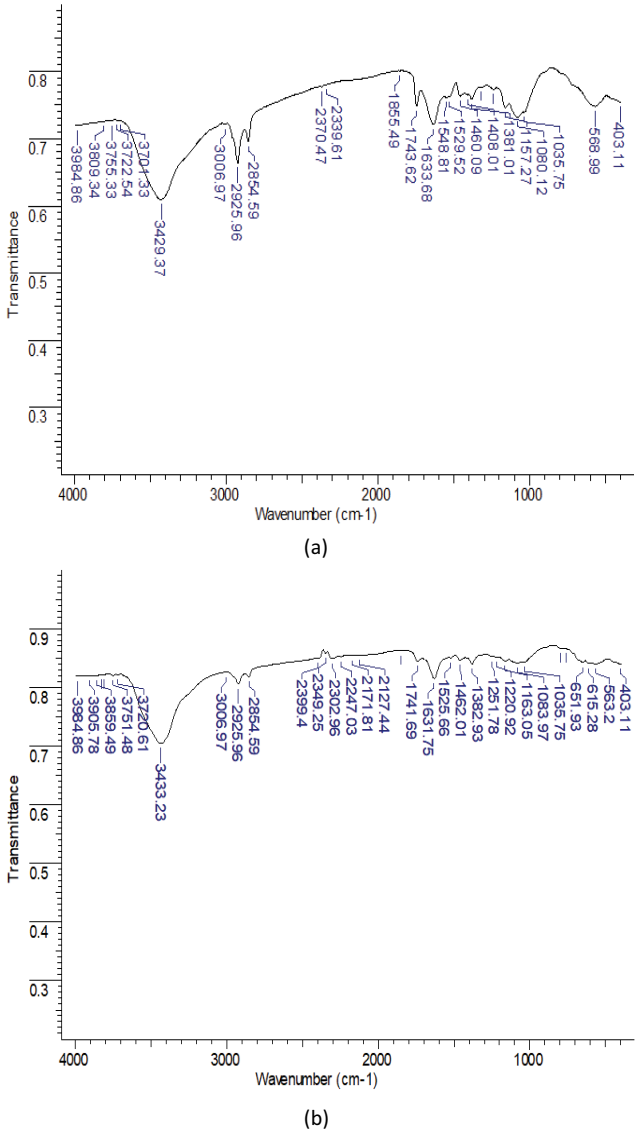

Fig. 5. FTIR profiles of untreated (a) and dye loaded (b) magnetic biosorbent.

depolarized hexagonal vibration after 1,500 cm^{-1}, are accordant with the literature. In the Raman analysis of $FeSO_4$, observation the characteristic SO_4 vibration at 1,018 cm^{-1}, the determination of the deuteration vibration at 973 cm^{-1} (normally at between 950 and 1,000 cm^{-1}), and the presence of symmetrical binding vibrations at 420–500 cm^{-1} confirm the magnetism [30–33]. After the biosorbent has been magnetized, the characteristic vibrations observed in $FeCl_3$ and $FeSO_4$ were previously characterized and observed again in the specified spectrum range. As a result, it has been determined that biosorbent becomes magnetic (Fig. 6).

In the Raman analysis obtained after adsorption process, a change in the structure of the biosorbents was observed. These findings are consistent with the literature. After the applied biosorption process, vibrations between 1,200 and 1,600 cm^{-1} related to magnetism was observed. Similar studies are included in the literature [34–37] (Fig. 6).

3.4.3. Zeta potential analysis

At low pH, the fungal biomass was more interested in binding to protonated binding sites, so it was observed that the capacity of biosorption of RO13 anionic dyestuff by #4 fungal biomass decreased with increasing pH (from pH 2 to 7) (Table 1). The binding affinity of the dyestuff molecule decreases because of the deprotonization of the functional groups (in which case the surface loads of the biosorbents are negative) with increasing pH value for both before and after magnetization of the fungal biomass studied. This is consistent with the zeta potential values of the magnetic fungal biosorbent given in Fig. 7. When the surface load results of magnetic fungal biomass are examined, isoelectronic point is observed around pH 3 according to zeta potential values taken in water. The binding sites and dye anions showed electrostatic interactions which was understood from the measurements of the zeta potential.

3.4.4. XRD analysis

The crystal phases of the magnetic fungal biosorbent were determined by XRD analyses before and after dye biosorption (Figs. 8a and b). The XRD patterns of the magnetic fungal biomass before and after the biosorption were determined by the six characteristic peaks of Fe_3O_4 ($2\theta = 30.45°$, 35.75°, 43.39°, 53.99°, 57.29°, and 62.94°; before biosorption) and ($2\theta = 30.38°$, 35.63°, 43.39°, 53.70°, 57.32°, and 63.10°; after biosorption). These peaks were also consistent with the database included in the MDI Jade 5.0X analysis program and showed that Fe_3O_4 particles were precipitated to the biosorbent surface. Similar results have been observed in the literature. In a study conducted by, Yu et al., cationic dye adsorption with magnetically modified beer yeast biomass was carried out and six peculiar peaks ($2\theta = 30.1°$, 35.5°, 43.3°, 53.4°, 57.2°, and 62.9°) indices [(220), (311), (400), (422), (511), and (440)] of XRD analysis of magnetic biomass were observed [38]. The results are consistent with other studies in the literature [39,40].

3.4.5. Surface area analysis

The surface areas of the untreated and dye loaded magnetic biosorbents were 7.88 and 23.25 m^2/g, respectively. On introduction of dye and MagMC surface, the specific surface area increased. Similar results have been observed by others [41]. This result suggests that the surface area increased as a result of a porous framework created from intercalation. Average pore radiuses were determined as 91.2 and 19.2 Å for untreated and after treated with dye, respectively. Average pore radius decreased with dye loading.

Fig. 9 shows the surface area analyses of untreated and dye loaded magnetic biosorbents. It appears fifth type isotherm line and it represents mesoporous structure of biosorbent. This type also indicates the initial capillary condensation after the surface is coated as monolayer [42].

3.4.6. SEM-EDX analysis

When EDX spectra of magnetic fungal biosorbent before (Fig. 10a) and after biosorption (Fig. 10b) were examined; high concentrations of iron peaks were observed. These results

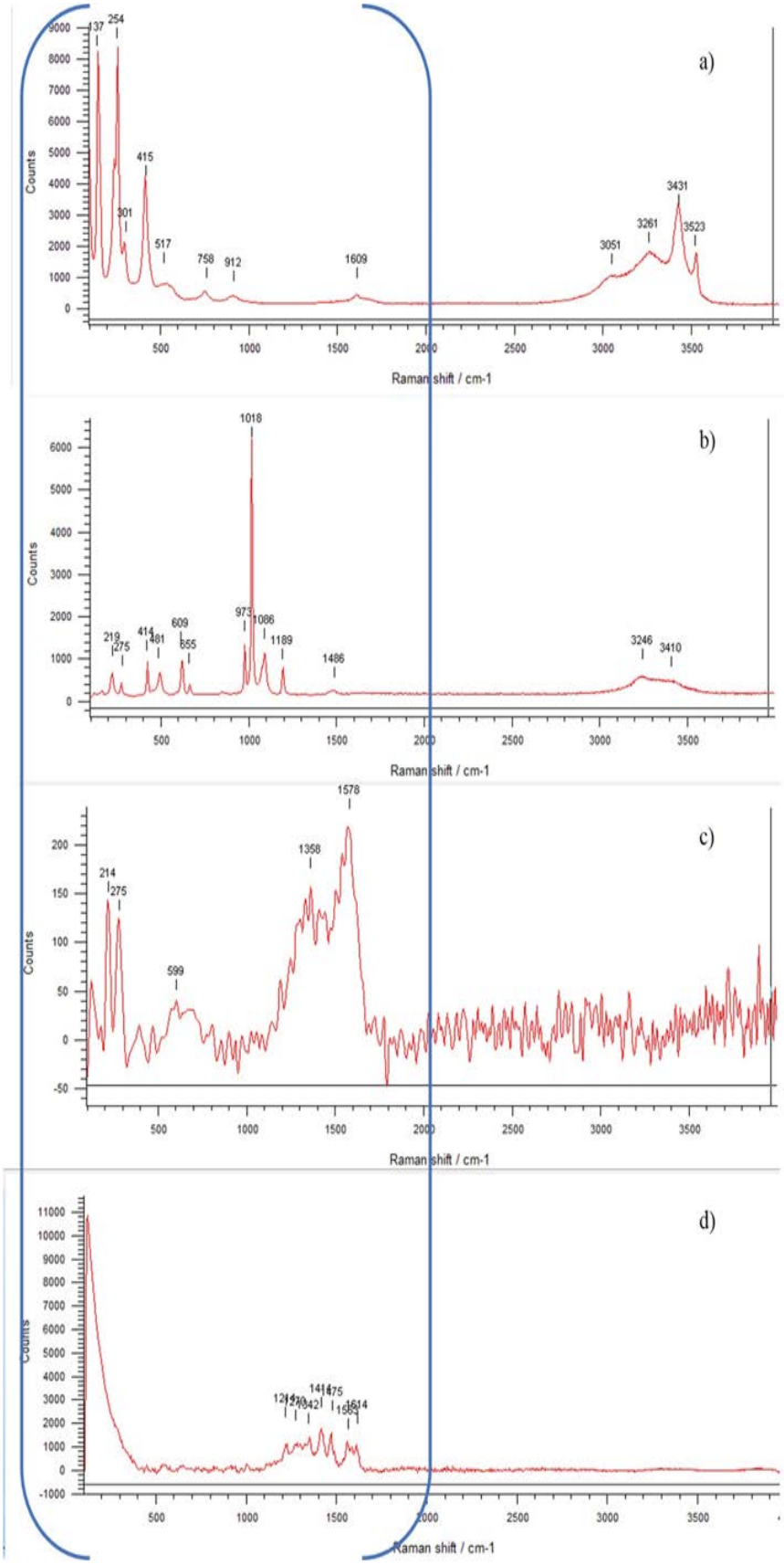

Fig. 6. Raman spectrum profiles (a) $FeSO_4$, (b) $FeCl_3$, (c) magnetic biosorbent, (d) dyestuff loaded magnetic biosorbent.

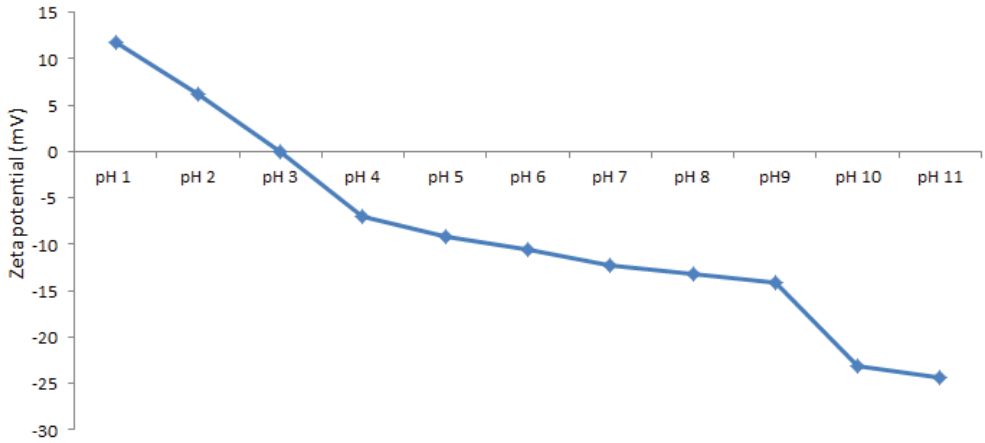

Fig. 7. Zeta potential measurement of the magnetic biosorbent.

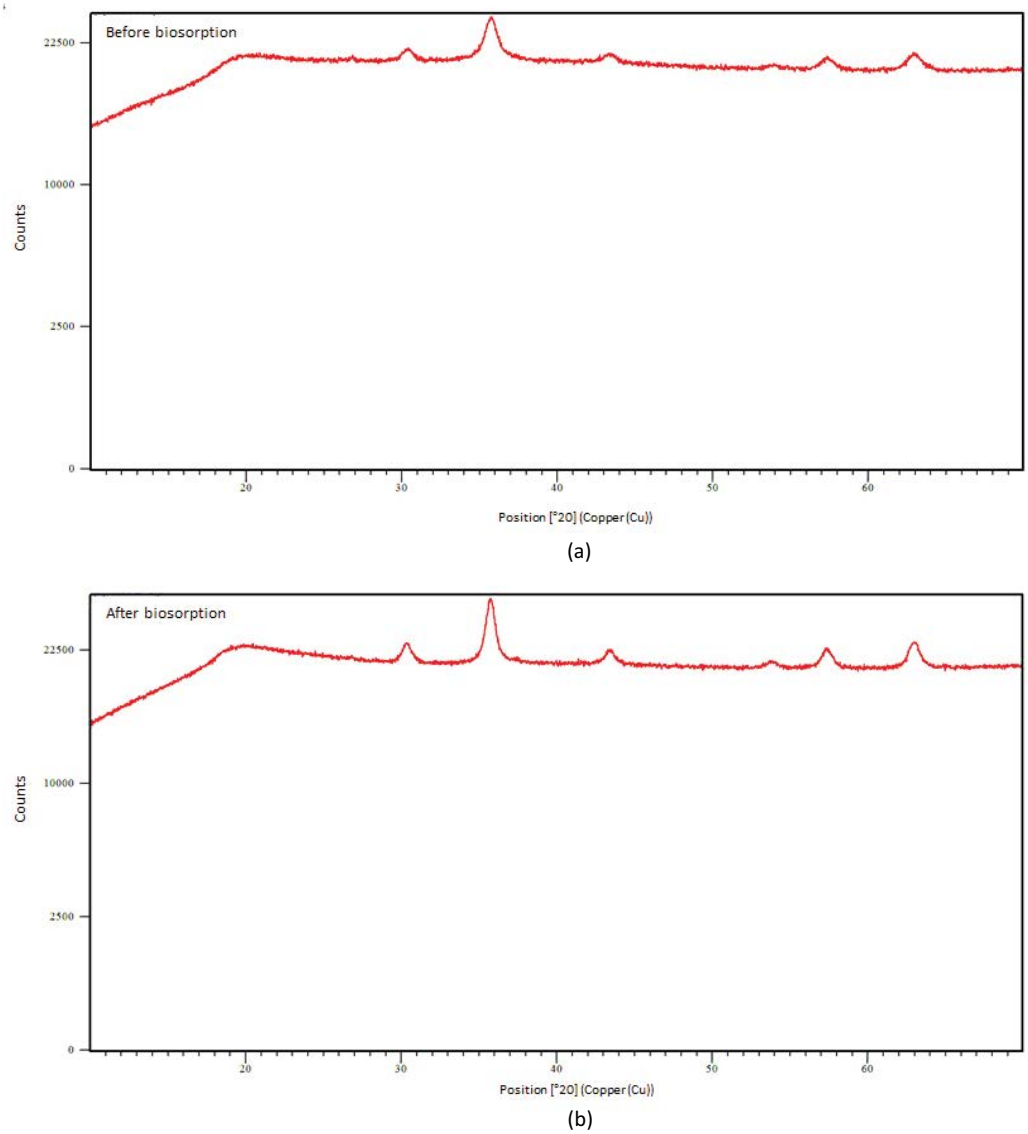

Fig. 8. XRD analyses of untreated (a) and dye loaded (b) magnetic biosorbents.

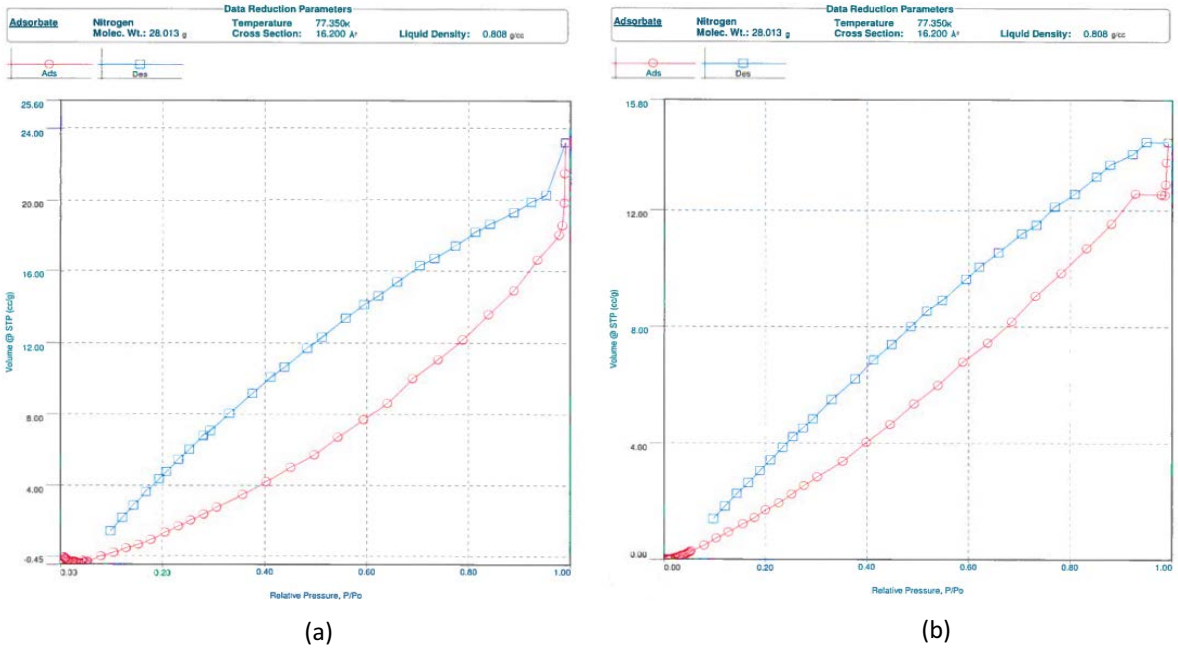

Fig. 9. Surface area analyses of untreated (a) and dye loaded (b) magnetic biosorbents.

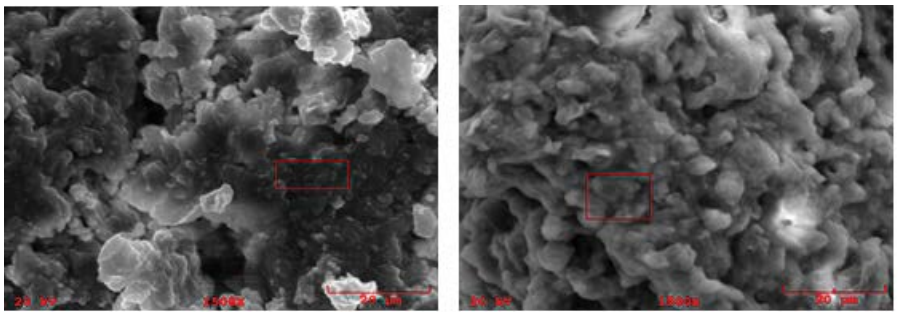

Comp.	Mole Conc.	Conc.	
Fe	17.494	46.747	
C	64.695	37.182	
O	14.217	10.884	
Mg	0.558	0.649	
P	2.859	4.237	
Cl	0.178	0.302	
	100.000	100.000	Total

(a)

Comp.	Mole Conc.	Conc.	
Fe	42.583	73.635	
C	37.686	14.015	
O	14.458	7.162	
P	2.673	2.563	
P	2.190	2.174	
S	0.410	0.451	
	100.000	100.000	Total

(b)

Fig. 10. SEM-EDS analysis of untreated (a) and dye loaded (b) magnetic biosorbents.

are other indication that the magnetic property of the biosorbent has been successfully introduced. Furthermore, magnetized fungal biosorbent contacted the RO13 dyestuff; a mechanism relating to iron ions on dye biosorption had no significant impact (Figs. 10a and b). However, the decrease of carbon amount of the dye loaded magnetic biosorbent was notable. This can be assumed to the formation of a complex between dye and carbon. This finding is consistent with the literature [43].

3.5. Biosorbent characterization

M. circinelloides (accession number: MN503306) was identified as the biosorbent that achieved dyestuff biosorption. Other studies have been reported about studying on bioremediation of heavy metals and biosorption of dyestuff [36,44,45], in which this microorganism previously was isolated from acid mine drainage, contaminated soil, and wastewater. However, microorganism was isolated

from mill scale being rich in iron(III) oxide in this study and *M. circinelloides* was successfully grown in malt broth with 5% of mill scale, water with 5% of mill scale, and only malt broth without pH adjustment.

The fungus from which the biosorbent used in this study was isolated from the mill scale containing 52% Fe_2O_3 and 29.46% C in terms of inorganic and organic contents, respectively. Due to the high iron concentration, this habitat can also be described as an extreme field. No information about microorganism isolation from mill scale has been found in the literature.

4. Conclusions

RO13 reactive textile dye efficiently removed from its aqueous solution with using magnetic biosorbent *M. circinelloides* (accession number: MN503306). Effect of various parameters on to biosorption efficiency was investigated and maximum biosorption capacity was obtained as 400 mg/g at 30°C, 240 ppm of initial dye concentration, 0.1 g/L of biosorbent dosage in reaction medium within 60 min. CCD method were used to optimize reaction conditions and ın optimum conditions, dye removal yield was found to be 95.765%. According to the kinetic and thermodynamic studies pseudo-second-order kinetic model and Langmuir isotherm model was found the best fitted, respectively, according to regression coefficients. Thermodynamic parameters have revealed that the adsorption process is spontaneous and endothermic in nature.

As a conclusion, the biomass of *M. circinelloides* has a great potential for application in biological treatment of industrial effluents from dye industry. This report is the first that demonstrates the efficient adsorption of reactive dyestuffs by a fungus isolated from iron-rich oily mill scale. Further studies will focus on the removal of other hazardous materials to treat biologically.

Acknowledgments

This study was supported by Eskisehir Osmangazi University Scientific Research Projects Committee (Project no: 2019-2814).

References

[1] V.V. Priyan, T. Shahnaz, E. Suganya, S. Sivaprakasam, S. Narayanasamy, Ecotoxicological assessment of micropollutant Diclofenac biosorption on magnetic sawdust: phyto, microbial and fish toxicity studies, J. Hazard. Mater., 403 (2020) 123532 (1–13), doi: 10.1016/j.jhazmat.2020.123532.

[2] C. Patra, R. Gupta, D. Bedadeep, S. Narayanasamy, Surface treated acid-activated carbon for adsorption of anionic azo dyes from single and binary adsorptive systems: a detail insight, Environ. Pollut., 266 (2020) 115102 (R713–R715), doi: 10.1016/j.envpol.2020.115102.

[3] R. Sivashankar, A.B. Sathya, K. Vasantharaj, V. Sivasubramanian, Magnetic composite an environmental super adsorbent for dye sequestration – a review, Environ. Nanotechnol. Monit. Manage., 1–2 (2014) 36–49.

[4] B. Lellis, C.Z. Fávaro-Polonio, J.A. Pamphile, J.C. Polonio, Effects of textile dyes on health and the environment and bioremediation potential of living organisms, Biotechnol. Res. Innovation, 3 (2019) 275–290.

[5] J. Khatri, P.V. Nidheesh, T.A. Singh, M.S. Kumar, Advanced oxidation processes based on zero-valent aluminium for treating textile wastewater, Chem. Eng. J., 348 (2018) 67–73.

[6] I. Anastapoluos, A. Mittal, M. Usman, J. Mittal, G. Yu, A. Nugez-Delgado, M. Kornaros, A review on halloysite-based adsorbents to remove pollutants in water and wastewater, J. Mol. Liq., 269 (2018) 855–868.

[7] C. Arora, S. Soni, S. Sahu, J. Mittal, P. Kumar, P.K. Bajpai, Iron based metal organic framework for efficient removal of methylene blue dye from industrial waste, J. Mol. Liq., 284 (2019) 343–352.

[8] E.S. Bireller, P. Aytar, S. Gedikli, A. Cabuk, Removal of some reactive dyes by untreated and pretreated *Saccharomyces cerevisiae*, an alcohol fermentation waste, J. Sci. Ind. Res., 71 (2012) 632–639.

[9] A. Çabuk, P. Aytar, S. Gedikli, Y.K. Özel, E. Kocabıyık, Biosorption of acidic textile dyestuffs from aqueous solution by *Paecilomyces* sp. isolated from acidic mine drainage, Environ. Sci. Pollut. Res., 20 (2013) 4540–4550.

[10] P. Aytar, S. Gedikli, Y. Buruk, A. Cabuk, N. Burnak, Lead and nickel biosorption with a fungal biomass isolated from metal mine drainage: Box–Behnken experimental design, Int. J. Environ. Sci. Technol., 11 (2016) 1631–1640.

[11] A. Çabuk, S. Gedikli, P. Aytar, M. Çelikdemir, Color removal of reactive textile dyes from aqueous solution by raw and modified fungal biosorbent, Environ. Eng. Manage. J., 14 (2015) 2353–2363.

[12] P. Aytar, D. Bozkurt, S. Erol, M. Özdemir, A. Çabuk, Increased removal of Reactive Blue 72 and 13 acidic textile dyes by *Penicillium ochrochloron* fungus isolated from acidic mine drainage, Desal. Water Treat., 57 (2016) 19333–19343.

[13] Ş. Katar, S. Erol, P. Aytar Çelik, M. Özdemir, A. Çabuk, *Talaromyces aculeatus* from acidic environment as a new fungal biosorbent for removal of some reactive textile dyes, Anadolu Univ. J. Sci. Technol. A, 18 (2017) 521–534.

[14] M. Divriklioglu, S.T. Akar, T. Akar, A passively immobilized novel biomagsorbent for the effective biosorptive treatment of dye contamination, Environ. Sci. Pollut. Res., 26 (2019) 25834–25843.

[15] M. Hassan, R. Naudi, J. Du, Y. Liu, F. Qi, Critical review of magnetic biosorbents: their preparation, application, and regeneration for wastewater treatment, Sci. Total Environ., 102 (2020) 134893 (1–21), doi: 10.1016/j.scitotenv.2019.134893.

[16] A.C. Khorasani, S.A. Shojaosadati, Magnetic pectin-*Chlorella vulgaris* biosorbent for the adsorption of dyes, J. Environ. Chem. Eng., 7 (2019) 103062 (1–8), doi: 10.1016/j.jece.2019.103062.

[17] S.F. Soares, T. Fernandes, T. Trindade, A.L. Daniel-da-Silva, Recent advances on magnetic biosorbents and their applications for water treatment, Environ. Chem. Lett., 18 (2020) 151–164.

[18] D. Mehta, S. Mazumdar, S.K. Singh, 2015 Magnetic adsorbents for the treatment of water/wastewater—a review, J. Water Process. Eng., 7 (2015) 244–265.

[19] C. Su, Environmental implications and applications of engineered nanoscale magnetite and its hybrid nanocomposites: a review of recent literature, J. Hazard. Mater., 322 (2017) 48–84.

[20] M. Safarikova, L. Ptackova, I. Kibrikova, I. Safarik, Biosorption of water-soluble dyes on magnetically modified *Saccharomyces cerevisiae* subsp. *uvarum* cells, Chemosphere, 59 (2005) 831–835.

[21] V.I. Shatokha, O.O. Gogenko, S.M. Kripak, Utilising of the oiled rolling mill scale in iron ore sintering process, Resour. Conserv. Recycl., 55 (2011) 435–440.

[22] D. Paswan, M. Malathi, R.K. Minj, D. Bandopadhyay, Mill scale: a potential raw material for iron and steel making, Stainless Steel World, 21 (2015) 54–56.

[23] C. Li, X. Wang, D. Meng, L. Zhou, Facile synthesis of low-cost magnetic biosorbent from peach gum polysaccharide for selective and efficient removal of cationic dyes, Int. J. Biol. Macromol., 107 (2018) 1871–1878.

[24] P. Panneerselvam, N. Morad, K.A. Tan, Magnetic nanoparticle (Fe_3O_4) impregnated onto tea waste for the removal of nickel(II) from aqueous solution, J. Hazard. Mater., 186 (2011) 160–168.

[25] S.S. Gupta, K.G. Bhattacharyya, Removal of Cd(II)from aqueous solution by kaolinite, montmorillonite and their poly(oxo

zirconium) and tetrabutylammonium derivatives, J. Hazard. Mater., 128 (2006) 247–257.
[26] S.A. Khan, R. Rehman, M.A. Khan, Adsorption of chromium(III), chromium(VI) and silver(I) on bentonite, Waste Manage., 15 (1995) 271–282.
[27] B.Y. Gürsu, P. Aytar Çelik, S. İlhan, Y.E. Kocabıyık, S. Gedikli, A. Çabuk, Diversity of microfungi in acid mine drainages, BioDiCon, 10 (2017) 184–192.
[28] M.M. Areco, A. Hanela, J. Duran, M.S. Afonso, Biosorption of (Cu(II) and Pb) by dead biomasses of green alga *Ulva lactuca* and the development of a sustainable matrix for adsorption, J. Hazard. Mater., 213–214 (2012) 123–132.
[29] Q. Li, M. Wang, X. Yuan, D. Li., H. Xu, L. Sun, F. Pan, D. Xia, Study on the adsorption and desorption performance of magnetic resin for Congo red, Environ. Technol., 42 (2021) 1552–1559.
[30] A. Givan, A. Loewenschuss, Matrix isolation Raman spectra of $FeCl_3$ and Fe_2Cl_6, J. Raman Spectrosc., 6 (1977) 84–88.
[31] N. Coswell, S.A. Solin, Vibrational excitations of pure $FeCl_3$ and graphite intercalated with ferric chloride, Solid State Commun., 27 (1978) 961–967.
[32] M. Sitze, E.R. Schreiter, E.V. Patterson, G. Freeman, Ionic liquids based on $FeCl_3$ and $FeCl_2$ Raman Scattering and ab Initio calculations, Inorg. Chem., 40 (2001) 2298–2304.
[33] C.H. Chio, S.K. Sharma, D.W. Muenow, The hydrates and deuterates of ferrous sulfate ($FeSO_4$): a Raman spectroscopic study, J. Raman Spectrosc., 38 (2007) 87–99.
[34] Z. Ren, X. Xu, X. Wang, B. Gao, Q. Yue, W. Song, L. Zhang, H. Wang, FTIR, Raman, and XPS analysis during phosphate, nitrate and Cr(VI) removal by amine cross-linking biosorbent, J. Colloid Interface Sci., 468 (2016) 313–323.
[35] E. Makhado, S. Pandey, J. Ramontja, Microwave assisted synthesis of xanthan gum-cl-poly(acrylic acid) based-reduced graphene oxide hydrogel composite for adsorption of methylene blue and methyl violet from aqueous solution, Int. J. Biol. Macromol., 119 (2018) 255–269.
[36] E. Azin, H. Moghimi, Efficient mycosorption of anionic azo dyes by *Mucor circinelloides*: surface functional groups and removal mechanism study, J. Environ. Chem. Eng., 6 (2018) 4114–4123.
[37] R. Foroutan, R. Mohammadi, J. Razeghi, B. Ramavandi, Performance of algal activated carbon/Fe_3O_4 magnetic composite for cationic dyes removal from aqueous solutions, Algal Res., 40 (2019) 101509 (1–12), doi: 10.1016/j.algal.2019.101509.
[38] J.X. Yu, L.Y. Wang, R.A. Chi, Y.F. Zhang, Z.G. Xu, J.A. Guo, Simple method to prepare magnetic modified beer yeast and its application for cationic dye adsorption, Environ. Sci. Pollut. Res., 20 (2013) 543–551.
[39] Q.Q. Peng, Y.G. Liu, G.M. Zeng, W.H. Xu, C.P. Yang, J.J. Zhang, Biosorption of copper(II) by immobilizing *Saccharomyces cerevisiae* on the surface of chitosan-coated magnetic nanoparticles from aqueous solution, J. Hazard. Mater., 177 (2010) 676–682.
[40] Y.W. Chen, J.L. Wang, Preparation and characterization of magnetic chitosan nanoparticles and its application for Cu(II) removal, Chem. Eng. J., 168 (2011) 286–292.
[41] Y.S. Ho, G. McKay, The sorption of lead(II) ions on peat, Water Res., 33 (1999) 578–584.
[42] Y. Sarıkaya, Fizikokimya, 11th ed., Gazi Press, Ankara, Turkey, 2004, pp. 638–640.
[43] G. Cengiz, P. Aytar, M. Şam, A. Çabuk, Removal of reactive dyes using magnetically separable *Trametes versicolor* cells as a new composite biosorbent, Sep. Sci. Technol., 49 (2014) 1860–1871.
[44] Z. Cui, X. Zhang, H. Yang, L. Sun, Bioremediation of heavy metal pollution utilizing composite microbial agent of *Mucor circinelloides*, *Actinomucor* sp. and *Mortierella* sp., J. Environ. Chem. Eng., 5 (2017) 3616–3621.
[45] X. Zhang, H. Yang, Z. Cui, *Mucor circinelloides*: efficiency of bioremediation response to heavy metal pollution, Toxicol. Res., 6 (2017) 442–447.

Supplementary information

The mill scale primarily consists of iron oxides (about up to 70%–75%). Furthermore, this mill scale with high level of oil has negative environmental impacts and industrial disadvantages when the waste is recycled in the ironmaking and steelmaking process [18]. Minor element analysis and organic elemental (C/H/N/S) analysis of mill scale used in this study were performed by using X-ray fluorescence spectrometer (Panalytical ZETIUM) and C/H/N/S analyser (Perkin Elmer 2400 Series II), respectively and the results were presented in Table S1.

Table S1
Minor element and organic elemental analyses of mill scale industrial waste from which fungus isolation made

Minor elemental analysis (%)								
Loss of ignition	Fe_2O_3	Co_3O_4	Cr_2O_3	PbO	ZnO	TiO_2	NiO	CuO
35.370	52.053	0.106	0.066	0.056	0.658	0.070	0.104	0.061
SiO_2	P_2O_5	MnO	Al_2O_3	CaO	Na_2O	SO_3	K_2O	
3.349	0.550	1.122	1.868	3.709	0.410	0.386	0.063	
Organic elemental analysis (%)								
Carbon		Hydrogen		Nitrogen		Sulfur		
29.46		4.49		0.32		0.62		